ORIGINAL RESEARCH

Repeatability and Reproducibility of pseudo-Continuous Arterial Spin Labeling Measured Brain Perfusion in Healthy Volunteers and Glioblastoma Patients

Limin Zhou, Durga Udayakumar, Yiming Wang, Marco C. Pinho, Benjamin C. Wagner, Michael Youssef, Joseph A. Maldjian, Ananth J. Madhuranthakam

ABSTRACT

BACKGROUND AND PURPOSE: Arterial spin labeled (ASL) MRI has gained recognition as a quantitative perfusion imaging method for managing patients with brain tumors. Limited studies have so far investigated the reproducibility of ASL-derived perfusion in patients with brain tumors. This study aims to evaluate intrasession repeatability and intersession reproducibility of perfusion measurements using 3D pseudo-continuous ASL (pCASL) with Cartesian TSE (TSE-CASPR) in healthy volunteers (HV) and glioblastoma (GBM) patients at 3 Tesla and compare against 3D pCASL with GRASE.

MATERIALS AND METHODS: This prospective study (NCT03922984) was approved by the institutional review board and written informed consent was obtained from all subjects. HV underwent repeated pCASL evaluations 2-4 weeks apart between November 2021 and October 2022. GBM patients were recruited for longitudinal MRI from September 2019 to February 2023. Intrasession repeatability (HV and GBM) and intersession reproducibility (HV only) of pCASL were assessed using linear regression, Bland–Altman analyses, intraclass correlation coefficient (ICC) with 95% confidence interval (CI), and within-subject coefficients of variation (wsCV).

RESULTS: Twenty HV (9 men, age: 25.1±1.7 years, range 23-30 years) and 21 GBM patients (15 men; age: 59.8±14.3 years, range 28-81 years) were enrolled. Within imaging session, 3D pCASL measured perfusion with TSE-CASPR and GRASE respectively achieved high R^2 values (0.88–0.95; 0.93–0.96), minimal biases (-0.46 to 0.81; -0.08 to 0.35 mL/100g/min), high ICC [95% CI] (0.96-0.98 [0.94-0.98]; 0.96-0.98 [0.92-0.99]), and low wsCV (6.64%-9.07%; 5.20%-8.16%) in HV (N=20) and GBM patients (N=21). Across imaging session, 3D pCASL in HV (N=20) achieved high R^2 values (0.71; 0.82), minimal biases (-1.2; -0.90 mL/100g/min), high ICC [95% CI] values (0.85 [0.81-0.89]; 0.90 [0.87-0.93]), and low wsCV values (13.82%; 9.98%).

CONCLUSIONS: Our study demonstrated excellent intrasession repeatability of 3D pCASL measured cerebral perfusion in HV and GBM patients and good to excellent intersession reproducibility in HV. 3D pCASL with GRASE performed slightly better than 3D pCASL with TSE-CASPR in HV; however, in GBM patients, 3D pCASL with TSE-CASPR showed better performance in tumor regions with nearly twofold higher SNR. ASL measured perfusion could serve as a non-contrast quantitative imaging biomarker to facilitate the management of GBM patients.

ABBREVIATIONS: ASL = arterial spin labeling; pCASL = pseudo-continuous arterial spin labeling; GBM = glioblastoma; CBF = cerebral blood flow; CASPR = Cartesian acquisition with spiral profile reordering; GRASE = gradient and spin echo; NAGM = normal-appearing gray matter.

Received month day, year; accepted after revision month day, year.
From the Department of Radiology (L.Z., D.U., Y.W., M.C.P., B.C.W, J.A.M, A.J.M) and Department of Neurology (M.Y.), UT Southwestern Medical Center; Dallas, TX, USA.
Current address: Philips Healthcare (L.Z.), Cambridge, MA, USA; Department of Radiology (D.U., A.J.M.), Mayo Clinic, Rochester, MN, USA; Bayer Healthcare (Y.W.), Guangzhou, China.

The authors declare no conflicts of interest related to the content of this article.

Please address correspondence to Ananth J. Madhuranthakam, PhD, Department of Radiology, Mayo Clinic, 200 First Street SW, Rochester, MN, 55905, USA; email: ananth@mayo.edu

SUMMARY SECTION

PREVIOUS LITERATURE: Previous studies have demonstrated the value of ASL measured perfusion in various neurological conditions, showing potential for clinical use. While many studies have reported reliable and reproducible ASL perfusion measurements in healthy subjects, there has been a scarcity of such research in patient populations. Some studies have shown notable intrasession repeatability and moderate test-retest reproducibility of ASL in elderly patients with mild cognitive impairment and Alzheimer's disease. Nonetheless, studies that systematically investigated the reproducibility of ASL measured perfusion in patients with brain tumors have been limited.

KEY FINDINGS: Within imaging session in healthy volunteers (N=20) and glioblastoma (GBM) patients (N=21), and across imaging sessions in healthy volunteers (N=20), 3D pCASL measured perfusion with Cartesian TSE (TSE-CASPR) and GRASE achieved high R^2

values, minimal biases, high intraclass correlation coefficients, and low within-subject coefficients of variation.

KNOWLEDGE ADVANCEMENT: 3D pCASL with GRASE performed slightly better than 3D pCASL with TSE-CASPR in healthy volunteers. In GBM patients, however, 3D pCASL with TSE-CASPR showed better performance in tumor regions with nearly twofold higher SNR, bolstering 3D pCASL with TSE-CASPR as a quantitative non-contrast perfusion imaging biomarker in brain tumors.

INTRODUCTION

The utilization of quantitative imaging (QI) in radiology is gaining popularity for its improved precision in diagnosis, prognosis, and evaluating therapy response.[1] QI provides objective measurements, aiding in identifying subtle and sometimes qualitatively imperceptible changes in disease conditions. QI enables the correlation of accurately and precisely derived image metrics with relevant anatomical and physiological parameters, encompassing treatment effects and patient outcomes. A critical factor for the clinical adoption of QI is the demonstration of consistent repeatability and reproducibility of QI metrics, not only in healthy individuals but also in patient populations.

QI has shown significant promise in evaluating response to treatment in cancers.[2] Conventional radiological methods, such as the Response Evaluation Criteria in Solid Tumors (RECIST)[3] or the modified Response Assessment in Neuro-Oncology (RANO),[4,5] primarily focus on measuring tumor size changes. However, these conventional techniques may not detect early therapy responses, as many cancer treatments initially affect tumors at a microscopic level before any significant change in size becomes evident. QI techniques can identify these early effects, providing a valuable window of opportunity to effectively manage cancer treatments. Notably, angiogenesis, a key biological process that promotes aberrant tumor neovascularization,[6] is emerging as a vital perfusion imaging biomarker. Among all perfusion weighted imaging techniques, arterial spin labeled (ASL) magnetic resonance imaging (MRI)[7,8] has certain advantages. ASL MRI is a non-contrast and non-invasive imaging method that provides absolute quantitative measures of perfusion, proven to be especially valuable in brain imaging.

Based upon the recommendations from the International Society for Magnetic Resonance in Medicine (ISMRM) ASL expert panel, the early clinical adoption of ASL used 3D segmented acquisition techniques like 3D stack-of-spirals with multiple refocusing pulses or 3D gradient and spin echo (GRASE) for brain imaging.[9] Both acquisition methods, however, tend to suffer from image distortions in regions with increased B0 inhomogeneities.[10] This issue is particularly pertinent in patients with glioblastoma (GBM), an aggressive brain tumor, especially those who have undergone craniotomy, those with pre or post treatment intra-tumoral hemorrhage, and those located close to the skull base. To address this, alternate methods were developed using 3D turbo spin echo (TSE) using Cartesian acquisition with pseudo-continuous ASL (pCASL) for robust non-contrast perfusion imaging with minimized image distortions.[11-13] The purpose of this study was to evaluate intrasession repeatability and intersession reproducibility of perfusion measurements using 3D pCASL with Cartesian TSE in healthy volunteers and GBM patients at 3 Tesla and compare against 3D pCASL with GRASE.

MATERIALS AND METHODS

Participants

This prospective, single-institution study (ClinicalTrials.gov Identifier: NCT03922984) was approved by the institutional review board and written informed consent was obtained prior to the subject participation in the study. Healthy volunteer cohort: Twenty subjects who had no contraindications to standard MRI were enrolled between November 2021 and October 2022 (Table 1). Subjects with pregnancy or any history of neurological or psychiatric diseases were excluded. GBM study cohort: Twenty-one subjects with GBM were enrolled between September 2019 and February 2023 as part the clinical study (Table 1). The inclusion criteria were histologically proven GBM, no prior treatment such as chemotherapy, radiation treatment, or anti-angiogenic therapy except for surgery, and planned receipt of chemoradiation therapy. Since this is a repeatability and reproducibility study performed using repeated measurements at multiple visits, the methodology proposed in the Strengthening the Reporting of Observational Studies in Epidemiology (STROBE) checklist was followed.

Table 1: Demographic characteristics of healthy volunteers and patients with glioblastoma (GBM) included in the study analysis.

Sample Characteristics	Healthy Volunteers (n=20)	GBM Patients (n=21)
Male	9 (45%)	15 (71.4%)
Age, years (mean [SD])	25.1 (1.7)	59.8 (14.3)
Age range, years	23 – 30	28 – 81

MR Imaging Protocol

All imaging sessions were performed on a 3T MR scanner (Ingenia, Philips Healthcare) using a 32-channel head coil. All healthy volunteers were scanned twice with intersession time intervals of 2 to 4 weeks (Fig. 1A, top), matching the interval between the first two MRI time points of GBM patients (Fig. 1A, bottom). For each visit, two imaging sessions were performed with a 15-min break in between (Supplementary Figure 1A). In each imaging session, two runs of 3D pCASL with TSE using Cartesian acquisition with spiral profile reordering (CASPR)[11] and two runs of 3D pCASL with GRASE were performed. GBM patients were enrolled for longitudinal MR scans before, during, and after chemoradiation treatment, according to the clinical study (Fig. 1A, bottom). Each imaging session for GBM patients followed the recommended Brain Tumor Imaging Protocol (BTIP),[14] with additional sequences including two runs of 3D pCASL

with TSE-CASPR and at least one run of 3D pCASL with GRASE (Supplementary Figure 1B). All ASL acquisitions were performed before the administration of gadolinium-based contrast agent.

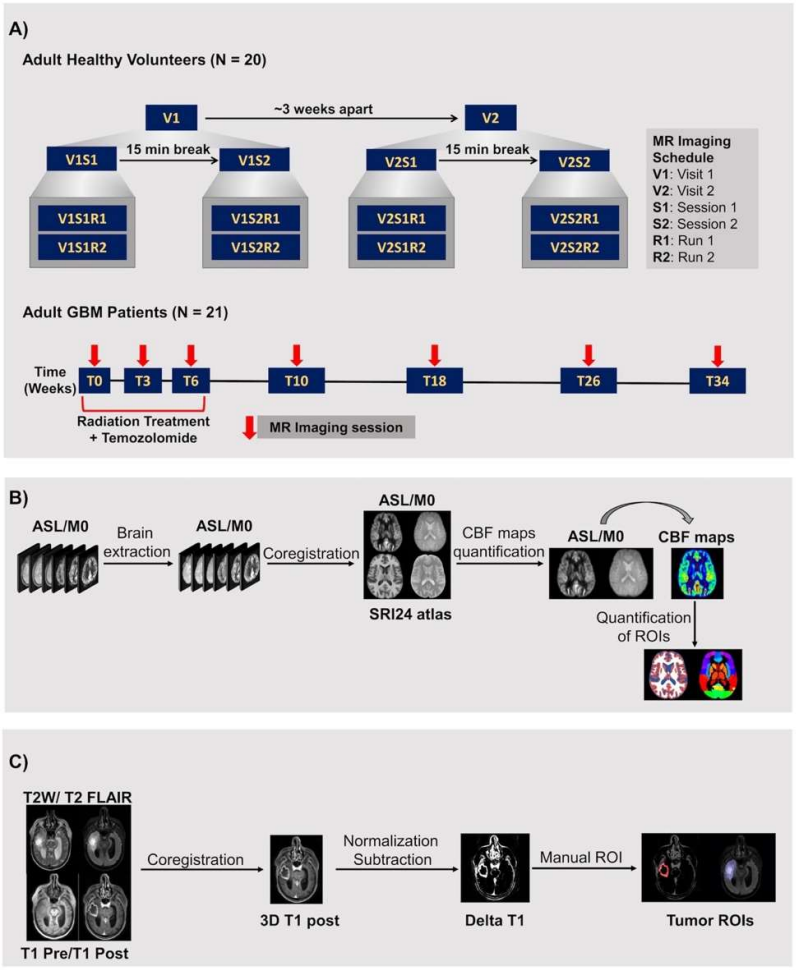

FIG 1. MR scan timelines and post-processing analysis pipelines for both healthy volunteers and patients with glioblastoma. A) MR scan timelines. Top: Each healthy volunteer participated in two visits (V1 and V2) with a time interval of 2 to 4 weeks. At each visit, there were two imaging sessions (S1 and S2) performed with a 15-minute break. Two runs (R1 and R2) of 3D pCASL with TSE-CASPR and two runs of 3D pCASL with GRASE were obtained in each imaging session with the imaging protocol shown in supplementary Figure 1A. Bottom: Each GBM patient participated in longitudinal MRI performed before (T0), during (T3, T6), and after (T10, T18, T26, T34) chemoradiation treatment, where the number after "T" represents the number of weeks from the beginning of treatment. T3 and T6 had a ±1 week range while T10-T34 had a ±2 weeks range. In addition to the standard clinical protocol for GBM, MRI was performed with 2 runs of 3D pCASL with TSE-CASPR and at least one run of 3D pCASL with GRASE, as shown in the supplementary Figure S1B. **B) ASL post-processing pipeline.** DICOM images were first converted to NIfTI format. ASL difference images and proton density (M0) images were skull stripped for brain extraction, followed by co-registration to the SRI24 atlas, and cerebral blood flow (CBF) map calculation. Segmentations of grey matter, white matter, and regional ROIs from the SRI24 atlas were used to extract CBF measurements in healthy volunteers. **C) Structural MR post-processing pipeline.** For GBM patients, the ASL post-processing pipeline was the same as in healthy volunteers (B). All structural MR images were co-registered to 3D T1 post-contrast images and manual tumor ROIs were drawn by an experienced neuroradiologist (M.C.P.), followed by co-registration to the SRI24 atlas for tumor and normal appearing grey and white matter ROIs extraction.

ASL labeling was applied in an axial plane perpendicular to the cervical spine C2 to C3 area with label duration (LD) and post-label delay (PLD) of 1.8 seconds each. A combination of several saturation and inversion pulses was used for background suppression (BGS) followed by spatially selective inflow saturation to reduce post-labeled arterial signal in the major vessels. 3D pCASL with TSE-CASPR was acquired in an axial plane with the following parameters: FOV = 220×220×110 mm^3, matrix = 64×64 with 42 slices, acquired resolution = 3.5×3.5×6 mm^3, reconstructed resolution = 3×3×3 mm^3, TR/TE = 6000/14 ms, echo spacing = 2.8 ms, TSE factor = 80, shot duration = 235 ms, number of signal average (NSA) = 1, and acquisition time = 3:10 minutes. A proton-density weighted image (M0) was acquired using the same acquisition parameters but without labeling, BGS, or inflow saturation pulses in 1:30 minutes. For comparison, ASL images were also acquired using the vendor-supplied 3D pCASL with GRASE, matching the same acquisition parameters as 3D pCASL with TSE-CASPR, except for: TR/TE = 3955/14 ms, echo spacing = 14.1 ms, TSE factor = 19, EPI factor = 15, shot duration = 268 ms, NSA = 3, and acquisition time = 4:37 minutes (including the M0). Both 3D pCASL with TSE-CASPR and 3D pCASL with GRASE had similar acquisition times of ~4:40 minutes, including M0.

Image Analysis

For healthy volunteers, the entire ASL processing pipeline included format conversion from DICOM to NIfTI with dcm2nii,[15] followed by skull stripping using the brain extraction tool in FSL,[16-18] and co-registration to the SRI24 structural atlas[19] by ANTS[20] (Fig. 1B). After alignment, ASL cerebral blood flow (CBF) maps were calculated using the single compartment model according to the following equation[9]:

$$\mathrm{CBF} = 6000 \cdot \frac{\Delta M}{M_0} \cdot \frac{\lambda}{2\alpha T_1} \cdot \frac{e^{PLD/T_1}}{1 - e^{-LD/T_1}} \quad \mathrm{mL/100g/min}$$

where ΔM is the signal intensity of the perfusion difference image; λ is the blood brain partition coefficient (0.9); T1 is the longitudinal relaxation time of blood (1600 ms); PLD of 1800 ms; LD of 1800 ms; α is the net labeling efficiency of 0.6 including BGS.[11,21] Perfusion measurements were then extracted from the grey matter, white matter, and regional regions of interest (ROIs) based on the SRI24 atlas.

For GBM patients, all images were first co-registered to T1 post-contrast images (Fig. 1C). The T1 pre- and post-contrast images were then normalized based on the signal intensity histogram[22] and subtracted to generate Delta T1 images. Using the structural T2, T2-FLAIR, T1-pre, and Delta T1 images, ROIs of the tumor characteristics were manually drawn by an experienced neuroradiologist (M.C.P.) including enhancing tumor, tumor core, whole tumor, necrosis, resection cavity, cyst, and hemorrhage. Subsequently, all non-baseline images including ASL, M0, and corresponding tumor ROIs were co-registered to the baseline MR images using ANTS. The CBF values from the tumor ROIs and the normal appearing brain ROIs (by excluding the tumor ROIs) were extracted. The mean and standard deviation of CBF values in mL/100 g/min were tabulated.

Statistical Analysis

All statistical analyses were performed with Prism (GraphPad, San Diego, CA). The normality of mean perfusion values was tested using the D'Agostino & Pearson test, Anderson-Darling test, Shapiro-Wilk test, and the Kolmogorov-Smirnov test. A paired t-test was performed to evaluate the difference between mean perfusion values from 3D pCASL with TSE-CASPR and 3D pCASL with GRASE. The reproducibility was measured using linear regression, Bland–Altman analyses, and intraclass correlation coefficient (ICC). ICC estimates and their 95% confidence intervals (CI) were calculated using the SPSS statistical package (SPSS, Chicago, IL) based on a single-measurement, absolute-agreement, 2-way mixed-effects model. Within-subject coefficients of variation (wsCV), defined as the ratio of the standard deviation (SD) of the difference between repeated measurements to the mean of the repeated measurements, were also computed. Signal to noise ratio (SNR) was calculated in healthy volunteers using dual acquisitions (R1 and R2), according to the NEMA methodology:[23]

$$\mathrm{SNR} = \sqrt{2}.\frac{mean\ (R1 + R2)}{SD(R1 - R2)}$$

RESULTS

Healthy Volunteers

ASL perfusion maps were successfully acquired in all 20 healthy volunteers. Each healthy volunteer underwent two MR visits (V1, V2) with four imaging sessions (V1S1, V1S2, V2S1, and V2S2) for a total of 80 imaging sessions. Within each imaging session, two runs (R1, R2) of 3D pCASL with TSE-CASPR and two runs of 3D pCASL with GRASE were performed (Fig. 1A, top). The average perfusion maps across all 20 healthy volunteers acquired at run 1 within each imaging session (i.e., V1S1R1, V1S2R1, V2S1R1, and V2S2R1) and at run 2 within each imaging session (i.e., V1S1R2, V1S2R2, V2S1R2, and V2S2R2) showed good co-registration and similar perfusion values demonstrating qualitative intrasession repeatability for both 3D pCASL with TSE-CASPR and 3D pCASL with GRASE (Fig. 2 left). Similarly, the average perfusion maps across all 20 healthy volunteers acquired at visit 1 (i.e., V1S1R1, V1S1R2, V1S2R1, and V1S2R2) and at visit 2 (i.e., V2S1R1, V2S1R2, V2S2R1, and V2S2R2) demonstrated qualitative intersession reproducibility for both readouts (Fig. 2 right).

Quantitative analyses also showed similar results for both 3D pCASL with TSE-CASPR (Fig. 3A) and 3D pCASL with GRASE (Fig. 3B), evaluated using linear regression (top row) and Bland-Altman analyses (bottom row). The intrasession repeatability measures of 3D pCASL with TSE-CASPR were: slope (95% CI) of 0.94 (0.89-1.0), R^2 value of 0.88, ICC (95% CI) of 0.96 (0.94-0.97), wsCV of 7.21%, and a minimal bias of 0.81 mL/100g/min (Fig. 3A, Table 2). The corresponding intrasession repeatability measures of 3D pCASL with GRASE were: slope (95% CI) of 1.02 (0.98-1.05), R^2 value of 0.96, ICC (95% CI) of 0.97 (0.96-0.98), wsCV of 5.2%, and a minimal bias of 0.35 mL/100g/min (Fig. 3B, Table 2). Overall, 3D pCASL with both readouts showed excellent intrasession repeatability with 3D GRASE performing slightly better than 3D TSE-CASPR.

The intersession reproducibility measures of 3D pCASL with TSE-CASPR were: slope (95% CI) of 0.78 (0.70-0.85), R^2 value of 0.71, ICC (95% CI) of 0.85 (0.81-0.89), wsCV of 13.82%, and a minimal bias of -1.2 mL/100g/min (Fig. 3A, Table 2). The corresponding intersession reproducibility measures of 3D pCASL with GRASE were: slope (95% CI) of 0.89 (0.82-0.96), R^2 value of 0.82, ICC (95% CI) of 0.90 (0.87-0.93), wsCV of 9.98%, and a minimal bias of -0.9 mL/100g/min (Fig. 3B, Table 2). The intersession reproducibility was good to excellent for 3D pCASL with both readouts with 3D GRASE performing better than 3D TSE-CASPR. Similar behavior of good to excellent intrasession reliability was observed by both readouts at regional ROI levels, while the intersession reproducibility was moderate (Supplementary Table 1).

The CBF measurements from both readouts showed normal distributions across all healthy volunteers ($p>0.05$ for all 4 normality tests). The paired t-test for mean CBF values showed no significant differences between the two readouts (Supplementary Figure 2), for both intrasession repeatability ($p=0.91$) and intersession reproducibility ($p=0.32$).

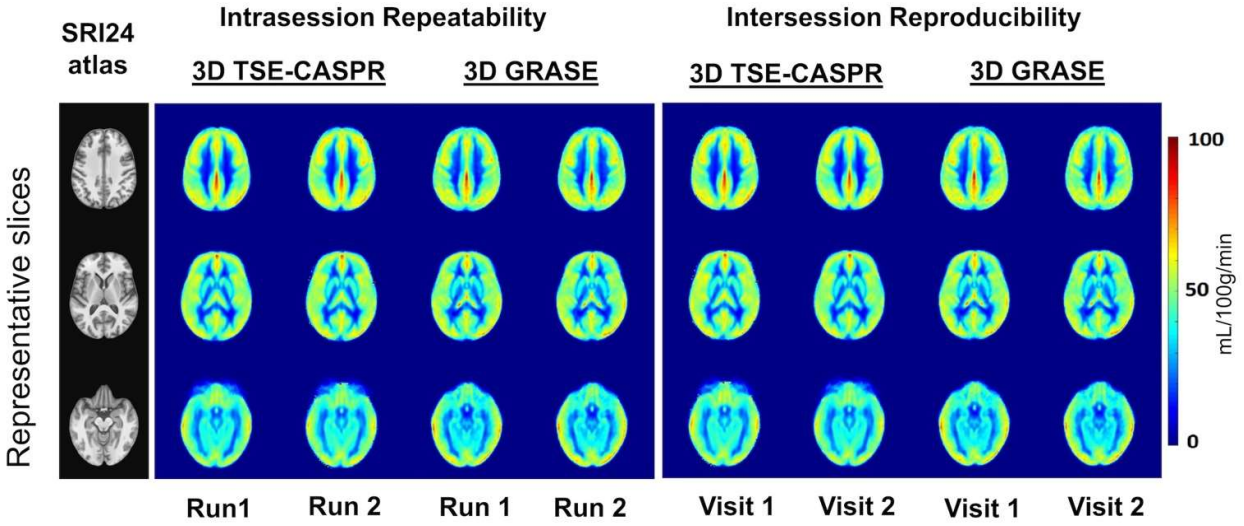

FIG 2. Co-registration between ASL measured perfusion maps and standard SRI24 atlas qualitatively shows good intrasession repeatability and intersession reproducibility in healthy volunteers. Representative slices of averaged perfusion maps among 20 healthy volunteers and corresponding SRI24 T1-weighted atlas slice for intrasession (left) and intersession (right) comparisons between two runs of 3D TSE-CASPR and 3D GRASE readouts. The unit of perfusion values are in mL/100g/min.

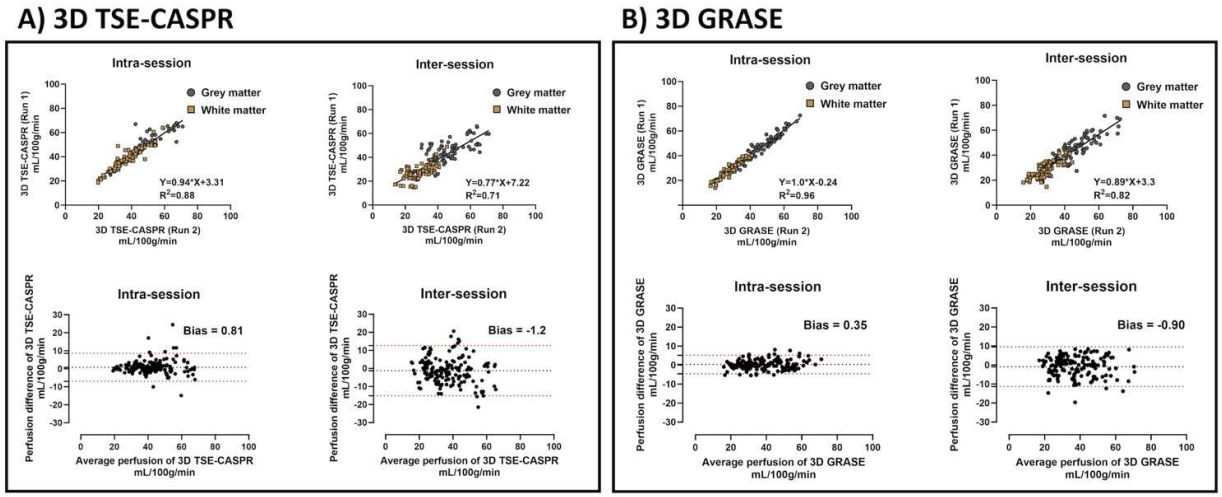

FIG 3. Quantitative analyses show good intrasession repeatability and intersession reproducibility of ASL measured perfusion in healthy volunteers. Linear regression (top) and Bland Altman analyses (bottom) in healthy volunteers. Mean perfusion values (ml/100g/min) in grey matter and white matter, measured using 3D pCASL with TSE-CASPR (left) and 3D pCASL with GRASE (right), were utilized for intrasession and intersession reproducibility evaluations.

Table 2: Statistical analyses demonstrate intrasession repeatability and intersession reproducibility of CBF measurements in healthy volunteers.

Linear Regression Analyses	Intra-session		Inter-session	
	Slope (95% CI)	R^2	Slope (95% CI)	R^2
3D TSE-CASPR	0.94 (0.89-1.00)	0.88	0.78 (0.70-0.85)	0.71
3D GRASE	1.02 (0.98-1.05)	0.96	0.89 (0.82-0.96)	0.82

Intra-Class Correlation Coefficient (ICC)	Intra-session		Inter-session	
	ICC (95% CI)	wsCV	ICC (95% CI)	wsCV
3D TSE-CASPR	0.96 (0.94-0.97)	7.21	0.85 (0.81-0.89)	13.82
3D GRASE	0.97 (0.96-0.98)	5.20	0.90 (0.87-0.93)	9.98

GBM Patients

Representative slices of perfusion maps covering the tumor along with corresponding structural MR images for one representative GBM patient are shown in Fig. 4 at multiple time points. All images demonstrated good co-registration across different time-points. The GBM patients were all treated with chemoradiation, which results in the adverse effect of global brain perfusion reduction over the duration of the therapy.[24,25] Hence, we limited our evaluation to only intrasession repeatability in GBM patients.

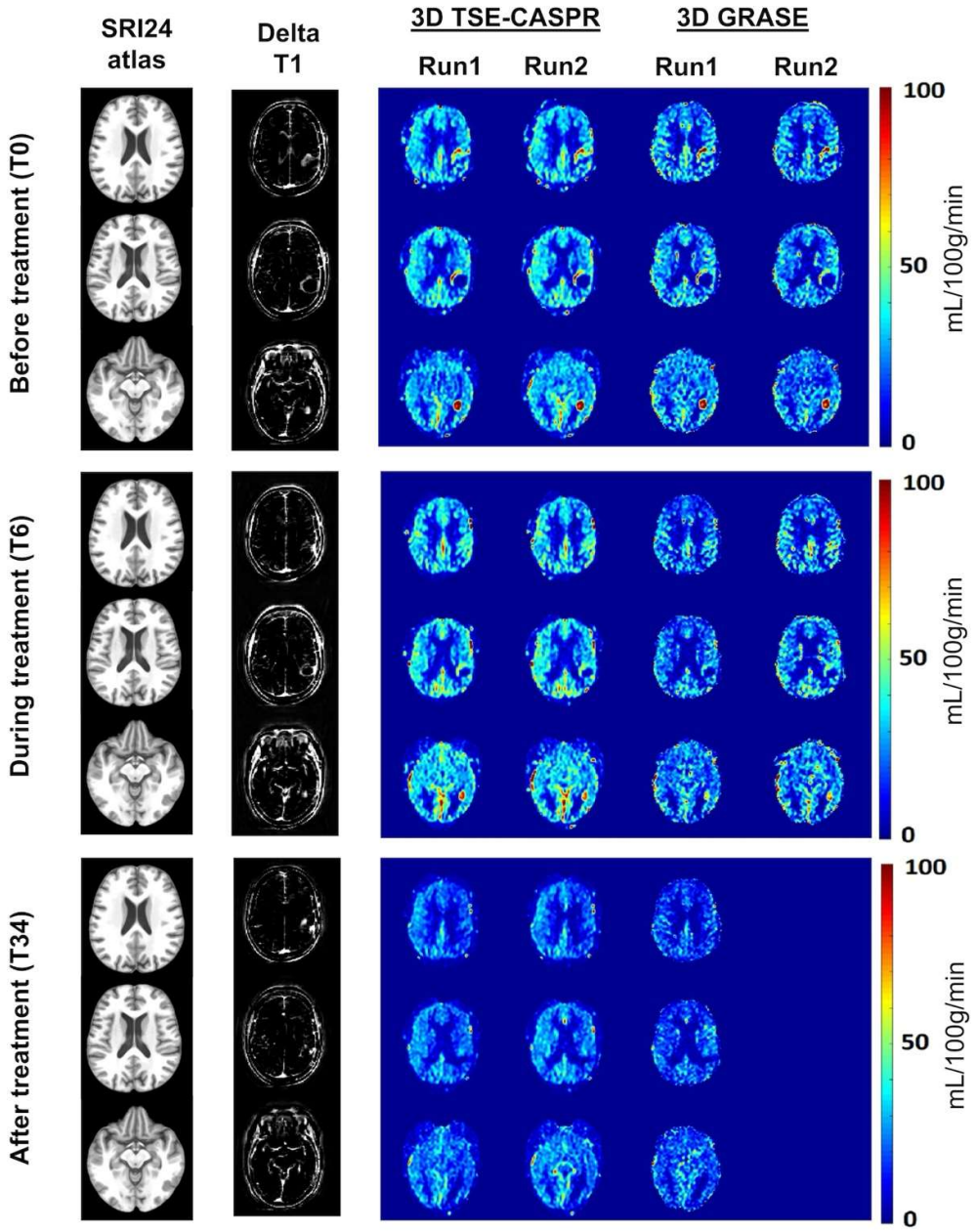

FIG 4. Significant reduction of global cerebral perfusion measurements in one GBM patient following chemoradiation, demonstrated by longitudinal MR scans. Representative slices of perfusion maps and corresponding structural MR images (SRI24 atlas slice and Delta T1) of a 71-year-old female GBM patient, shown at different time points before (top, T0), during (middle, T6) and after (bottom, T34) chemoradiation treatment. Two runs of 3D pCASL with TSE-CASPR were acquired for all three timepoints. Two runs of 3D pCASL with GRASE were performed for T0 and T6, while one run was performed at the T34 time point. The units of perfusion values are in mL/100g/min.

All 21 enrolled GBM patients underwent two runs of 3D pCASL with TSE-CASPR for a total of 88 imaging sessions. Across all 88 imaging sessions, linear regression and Bland-Altman analyses revealed excellent intrasession repeatability in both normal appearing brain regions (slope [95% CI] of 0.99 [0.95-1.02], R^2 value of 0.95, ICC [95% CI] of 0.98 [0.97-0.98], wsCV of 6.64%, and a minimal bias of -0.35 mL/100g/min) and in tumors (slope [95% CI] of 1.03 [0.97-1.09], R^2 value of 0.94, ICC [95% CI] of 0.97 [0.95-0.98], wsCV of 8.56%, and a minimal bias of -0.03 mL/100g/min) (Fig. 5, Table 3). Among the 21 GBM patients, 9 patients were also imaged with two runs of 3D pCASL with GRASE in addition to two runs of 3D pCASL with TSE-CASPR for a total of 32 imaging sessions. Hence, the intrasession repeatability comparison between the two readouts was performed in this sub-cohort analysis of 32 imaging sessions. Linear regression and Bland-Altman analyses revealed excellent intrasession repeatability for 3D pCASL with TSE-CASPR in both normal appearing brain regions (slope [95% CI] of 0.97 [0.90-1.03], R^2 value of 0.94, ICC [95% CI] of 0.97 [0.95-0.98], wsCV of 7.94%, and a minimal bias of -0.46 mL/100g/min) and in tumors (slope [95% CI] of 0.98 [0.89-1.07], R^2 value of 0.94, ICC [95% CI] of 0.97 [0.94-0.98], wsCV of 9.07%, and a minimal bias of -0.22 mL/100g/min) (Fig. 6A, Table 3). The corresponding intrasession repeatability for 3D pCASL with GRASE was also excellent in both normal appearing brain regions (slope [95% CI)] of 1.03 [0.95-1.10], R^2 value of 0.96, ICC [95% CI] of 0.98 [0.96-0.99], wsCV of 5.55%, and a minimal bias of -0.08 mL/100g/min) and in tumors (slope [95% CI)] of 0.94

[0.84-1.04], R^2 value of 0.93, ICC [95% CI] of 0.96 [0.92-0.98], wsCV of 8.16%, and a minimal bias of -0.06 mL/100g/min) (Fig. 6B, Table 3). Overall, the intrasession repeatability in GBM patients was excellent with both readouts in normal appearing brain regions, while the performance of 3D TSE-CASPR was slightly better in tumors compared to 3D GRASE.

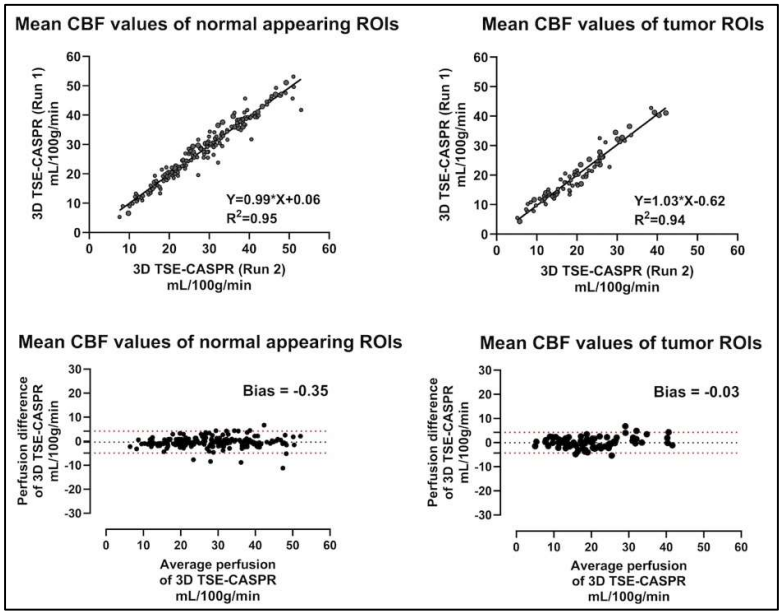

FIG 5. Quantitative analyses show good intrasession repeatability in tumor ROIs and normal appearing brain ROIs, for measured perfusion using 3D pCASL with TSE-CASPR among 21 GBM patients across 88 imaging sessions. Linear regression and Bland-Altman analyses were performed in GBM patients. Mean perfusion values (ml/100g/min) in tumor ROIs (left) and normal appearing grey matter and white matter (right), measured using 3D pCASL with TSE-CASPR, were used to evaluate intrasession reproducibility of ASL.

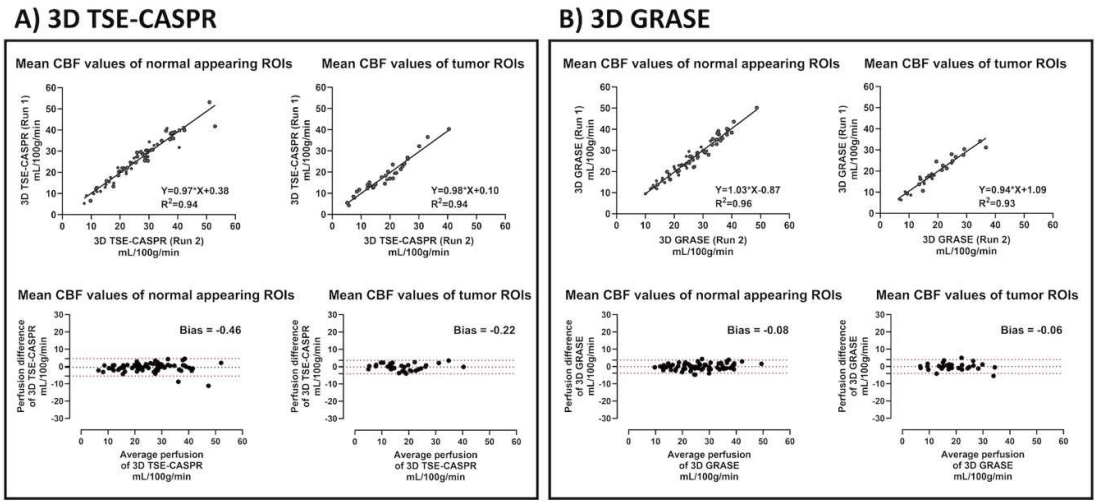

FIG 6. Comparison of quantitative analyses for ASL measured perfusion between 3D pCASL with TSE-CASPR and 3D pCASL with GRASE among 9 patients across 32 imaging sessions. Results shows good intrasession repeatability for both readouts in tumor ROIs and normal appearing brain ROIs of GBM patients. Linear regression and Bland-Altman analyses were performed in GBM patients. Mean perfusion values (ml/100g/min) in tumor ROIs (left) and normal appearing grey matter and white matter (right), measured using 3D pCASL with TSE-CASPR and 3D pCASL with GRASE, were used to evaluate intrasession reproducibility of ASL.

Table 3: Statistical analyses demonstrate intrasession repeatability of normal appearing grey and white matter and tumors in GBM patients.

Linear Regression Analyses	Tumor		Normal Appearing Gray/White Matter	
	Slope (95% CI)	R^2	Slope (95% CI)	R^2
3D TSE-CASPR (88 imaging sessions)	1.03 (0.97-1.09)	0.94	0.99 (0.95-1.02)	0.95
3D TSE-CASPR (32 imaging sessions only)	0.98 (0.89-1.07)	0.94	0.97 (0.90-1.03)	0.94
3D GRASE (32 imaging sessions)	0.94 (0.84-1.04)	0.93	1.03 (0.95-1.10)	0.96

Intra-Class Correlation Coefficient (ICC)	Tumor		Normal Appearing Gray/White Matter	
	ICC (95% CI)	wsCV	ICC (95% CI)	wsCV
3D TSE-CASPR (88 imaging sessions)	0.97 (0.95-0.98)	8.56	0.98 (0.97-0.98)	6.64
3D TSE-CASPR (32 imaging sessions only)	0.97 (0.94-0.98)	9.07	0.97 (0.95-0.98)	7.94
3D GRASE (32 imaging sessions)	0.96 (0.92-0.98)	8.16	0.98 (0.96-0.99)	5.55

3D TSE-CASPR has Higher SNR and Increased Robustness to Image Distortions than 3D GRASE

Figure 7 demonstrated the comparative image quality of perfusion maps acquired using 3D pCASL with TSE-CASPR and 3D pCASL with GRASE. In healthy volunteers, both readouts generated comparable quality perfusion maps without significant image distortions, as evident from the overlay on the anatomical T2-weighted images (Fig. 7A). However, in GBM patients, 3D TSE-CASPR provided more robust image quality and reduced image distortions compared to 3D GRASE, particularly in areas with increased B0 inhomogeneities as observed near surgical craniotomy locations (Fig. 7B). Similar behavior was also observed in healthy volunteers near areas with increased B0 inhomogeneities such as in the caudate, where 3D TSE-CASPR outperforms 3D GRASE in terms of intrasession repeatability and intersession reproducibility (Supplementary Table 1). CBF maps generated by 3D TSE-CASPR also demonstrated better tumor to normal background tissue contrast (Fig. 7B). Moreover, 3D TSE-CASPR had higher (~2 folds) SNR compared to 3D GRASE in grey matter (6.31±1.39 vs. 3.54±0.63, p<0.0001) and white matter (6.37±1.61 vs. 3.54±0.65, p<0.0001) (Fig. 7C).

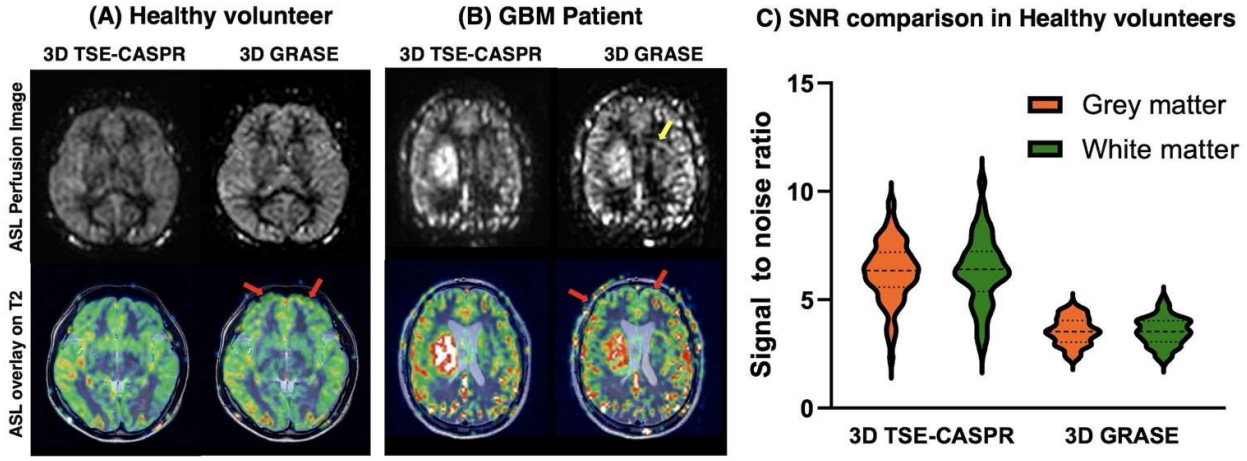

FIG 7. 3D TSE-CASPR has increased robustness to image distortions and higher SNR than that of 3D GRASE. A) Overlays of ASL images on T2 weighted structural images of a 25-years old female healthy volunteer with 3D TSE-CASPR on the left and 3D GRASE on the right. B) Overlays of ASL images on T2 weighted structural images of a 56-year-old male GBM patient with 3D TSE-CASPR on the left and 3D GRASE on the right. C) SNR values of ASL perfusion images using 3D pCASL with TSE-CASPR and 3D pCASL with GRASE, calculated with dual acquisitions across 20 healthy volunteers.

DISCUSSION

Arterial spin labeled (ASL) MRI has gained recognition as a quantitative imaging (QI) method for the measurement of cerebral blood flow (CBF), showing potential for diagnosis, response assessment and surveillance of brain tumor patients. For QI methods to be reliably adopted in clinical practice, high precision is essential. Our study has demonstrated excellent intrasession repeatability of 3D pCASL measured CBF in both healthy volunteers and GBM patients, evidenced by high R^2 values (TSE-CASPR: 0.88–0.95; GRASE: 0.93–0.96), minimal biases (TSE-CASPR: -0.46 to 0.81 mL/100g/min; GRASE: -0.08 to 0.35 mL/100g/min), high ICC [95% CI] values (TSE-CASPR: 0.96-0.98 [0.94-0.98]; GRASE: 0.96-0.98 [0.92-0.99]), and low wsCV values (TSE-CASPR: 6.64%-9.07%; GRASE: 5.20%-8.16%). Notably, this excellent repeatability was observed in both normal appearing brain regions and tumor ROIs for both TSE-CASPR and GRASE. Additionally, our study established good to excellent intersession reproducibility in healthy volunteers, as shown by high R^2 values (TSE-CASPR: 0.71; GRASE: 0.82), minimal biases (TSE-CASPR: -1.2 mL/100g/min; GRASE: -0.90 mL/100g/min), high ICC [95% CI] values (TSE-CASPR: 0.85 [0.81-0.89]; GRASE: 0.90 [0.87-0.93]), and low wsCV values (TSE-CASPR: 13.82%; GRASE: 9.98%). These findings strongly support the clinical translation of ASL as a non-contrast, noninvasive, and quality-controlled QI method for managing GBM patients.

Our data showed that 3D pCASL with GRASE performed slightly better than 3D pCASL with TSE CASPR for both intrasession repeatability and intersession reproducibility in healthy volunteers. In GBM patients, however, the performance of both readouts was equivalent in normal appearing regions, while 3D pCASL with TSE-CASPR showed slightly better performance in tumor ROIs. Our protocol acquired 3D GRASE with 3 NSAs and 3D TSE-CASPR with 1 NSA, maintaining equivalent acquisition times for both sequences. The better performance of 3D GRASE in healthy volunteers might be attributed to the averaging out of signal variations with increased NSAs. Conversely, 3D TSE-CASPR exhibited nearly twofold higher SNR, enhanced contrast between tumor and background tissue, improved robustness to B0 inhomogeneity, and fewer artifacts compared to 3D GRASE. These benefits likely contributed to the superior repeatability of 3D TSE-CASPR in GBM patients, particularly in tumor ROIs. Moreover, the increased resilience of 3D TSE-CASPR to

image distortions allows for precise co-registration of CBF maps to structural images such as T1, T2, and T2-FLAIR (e.g., Fig. 7B). This facilitates accurate tumor perfusion measurement using automated segmentations that are often performed using structural images. These advancements bring ASL closer to routine clinical use.

Previous studies have demonstrated that ASL can provide valuable perfusion information in various neurological conditions, showing potential for clinical use.[26,27] However, a significant hurdle has been the difficulty in achieving consistent ASL measured perfusion across different subjects and over time for the same subjects, which has hindered its clinical adoption. While many studies have reported reliable and reproducible ASL perfusion measurements in healthy subjects,[28,29] there has been a scarcity of such research in patient populations. Some studies have shown notable intrasession repeatability and moderate test-retest reproducibility of ASL in elderly patients with mild cognitive impairment and Alzheimer's disease.[30,31] Nonetheless, studies that systematically investigated the reproducibility of ASL measured perfusion in patients with brain tumors have been limited. Zhou et. al. has demonstrated high intrasession repeatability of pCASL measured perfusion in a small group of GBM patients, focusing on normal appearing grey matter and tumor regions.[32] Following this, Alsaedi et al.[33] has shown high repeatability for both pulsed ASL and pCASL for the assessment of perfusion parameters in a cohort of adult glioma patients. Our study corroborates these findings, showcasing high intrasession repeatability and intersession reproducibility of pCASL measured perfusion in both healthy volunteers and a larger group of GBM patients at multiple time points.

This study has several limitations. First, our healthy volunteers were relatively young (aged 23-30 years) compared to GBM patients (aged 28-81 years). Although major differences in the reproducibility of pCASL are not expected due to age, minor variations could still occur. Future studies will aim to align the age ranges of healthy volunteers with those of GBM patients to better facilitate clinical applicability. Second, pCASL sequences were acquired with a single PLD due to shorter scan time, ease of acquisition, post-processing, and clinical implementation. This single PLD may not be sufficient for accurate CBF quantification, especially in the elderly who may exhibit longer arterial transit times (ATT), including GBM patients. Nevertheless, ATTs are unlikely to change significantly within a single imaging session, thus not affecting intrasession repeatability. Similarly, ATT variations in healthy volunteers are not anticipated over short intervals (~3 weeks) and hence would not affect intersession reproducibility. Future studies will explore repeatability of 3D pCASL with multiple PLDs. Lastly, we did not assess intersession reproducibility in GBM patients due to the potential effects of chemoradiation therapy on normal brain regions. Future studies will consider normalization techniques and relative CBF measurements (34), similar to relative cerebral blood volume (rCBV) metrics used routinely in dynamic susceptibility contrast (DSC) imaging for brain tumors.[34]

CONCLUSIONS

In conclusion, our study demonstrated excellent intrasession repeatability of 3D pCASL measured cerebral perfusion in both healthy volunteers and GBM patients, along with good to excellent intersession reproducibility in healthy volunteers. Our study also demonstrated that 3D pCASL with GRASE performed slightly better than 3D pCASL with TSE-CASPR in healthy volunteers. In GBM patients, however, 3D pCASL with TSE-CASPR showed better performance in tumor regions with nearly twofold higher SNR. These findings bolster the potential of non-contrast, noninvasive, and quality-controlled ASL-measured perfusion particularly using 3D pCASL with TSE-CASPR as a QI biomarker in brain tumors. The application of ASL in clinical settings can aid in the diagnosis, prognosis, and the longitudinal assessment of treatment responses in managing GBM patients.

ACKNOWLEDGMENTS

This work was supported by NIH/NCI grants U01CA207091 and R01CA260705. The authors thank all volunteers and GBM patients for their time and consenting to participate in this study. The authors also thank Kelli Key, PhD, Michael Fulkerson, AS, LVN, Sydney Haldeman, MPH, Camille Harry, B.S., for their assistance with IRB and human subject recruitments; Abey Thomas, RT(MR), and Courtney Dawson, RT(MR), for their assistance in human imaging.

REFERENCES

1. Rosenkrantz AB, Mendiratta-Lala M, Bartholmai BJ, et al. Clinical utility of quantitative imaging. Acad Radiol 2015;22:33-49. PMC4259826.
2. Yankeelov TE, Mankoff DA, Schwartz LH, et al. Quantitative Imaging in Cancer Clinical Trials. Clin Cancer Res 2016;22:284-90. PMC4717912.
3. Eisenhauer EA, Therasse P, Bogaerts J, et al. New response evaluation criteria in solid tumours: revised RECIST guideline (version 1.1). Eur J Cancer 2009;45:228-47.
4. Wen PY, Chang SM, Van den Bent MJ, et al. Response Assessment in Neuro-Oncology Clinical Trials. J Clin Oncol 2017;35:2439-49. PMC5516482.
5. Ellingson BM, Wen PY, Cloughesy TF. Modified Criteria for Radiographic Response Assessment in Glioblastoma Clinical Trials. Neurotherapeutics 2017;14:307-20. PMC5398984.
6. Hanahan D, Weinberg RA. Hallmarks of cancer: the next generation. Cell 2011;144:646-74.
7. Detre JA, Leigh JS, Williams DS, et al. Perfusion imaging. Magn Reson Med 1992;23:37-45.
8. Williams DS, Detre JA, Leigh JS, et al. Magnetic resonance imaging of perfusion using spin inversion of arterial water. Proc Natl Acad Sci U S A 1992;89:212-6. 48206.

9. Alsop DC, Detre JA, Golay X, et al. Recommended implementation of arterial spin-labeled perfusion MRI for clinical applications: A consensus of the ISMRM perfusion study group and the European consortium for ASL in dementia. Magn Reson Med 2015;73:102-16. 4190138.
10. Li Z, Schar M, Wang D, et al. Arterial spin labeled perfusion imaging using three-dimensional turbo spin echo with a distributed spiral-in/out trajectory. Magn Reson Med 2016;75:266-73.
11. Greer JS, Wang X, Wang Y, et al. Robust pCASL perfusion imaging using a 3D Cartesian acquisition with spiral profile reordering (CASPR). Magn Reson Med 2019;82:1713-24. PMC6743738.
12. Taso M, Munsch F, Zhao L, et al. Regional and depth-dependence of cortical blood-flow assessed with high-resolution Arterial Spin Labeling (ASL). J Cereb Blood Flow Metab 2021;41:1899-911. PMC8327107.
13. Taso M, Zhao L, Guidon A, et al. Volumetric abdominal perfusion measurement using a pseudo-randomly sampled 3D fast-spin-echo (FSE) arterial spin labeling (ASL) sequence and compressed sensing reconstruction. Magn Reson Med 2019;82:680-92.
14. Ellingson BM, Bendszus M, Boxerman J, et al. Consensus recommendations for a standardized Brain Tumor Imaging Protocol in clinical trials. Neuro Oncol 2015;17:1188-98. PMC4588759.
15. Li X, Morgan PS, Ashburner J, et al. The first step for neuroimaging data analysis: DICOM to NIfTI conversion. J Neurosci Methods 2016;264:47-56.
16. Jenkinson M, Beckmann CF, Behrens TE, et al. Fsl. Neuroimage 2012;62:782-90.
17. Woolrich MW, Jbabdi S, Patenaude B, et al. Bayesian analysis of neuroimaging data in FSL. Neuroimage 2009;45:S173-86.
18. Smith SM, Jenkinson M, Woolrich MW, et al. Advances in functional and structural MR image analysis and implementation as FSL. Neuroimage 2004;23 Suppl 1:S208-19.
19. Rohlfing T, Zahr NM, Sullivan EV, et al. The SRI24 multichannel atlas of normal adult human brain structure. Hum Brain Mapp 2010;31:798-819. PMC2915788.
20. Avants BB, Tustison NJ, Stauffer M, et al. The Insight ToolKit image registration framework. Front Neuroinform 2014;8:44. PMC4009425.
21. Robson PM, Madhuranthakam AJ, Dai W, et al. Strategies for reducing respiratory motion artifacts in renal perfusion imaging with arterial spin labeling. Magn Reson Med 2009;61:1374-87. 2946256.
22. Nyul LG, Udupa JK, Zhang X. New variants of a method of MRI scale standardization. IEEE Trans Med Imaging 2000;19:143-50.
23. National Electrical Manufacturers Association - Determination of Signal-to-Noise Ratio (SNR) in Diagnostic Magnetic Resonance Imaging. March 31, 2021. at https://www.nema.org/Standards/view/Determination-of-Signal-to-Noise-Ratio-in-Diagnostic-Magnetic-Resonance-Imaging.)
24. Petr J, Hogeboom L, Nikulin P, et al. A systematic review on the use of quantitative imaging to detect cancer therapy adverse effects in normal-appearing brain tissue. MAGMA 2022;35:163-86. PMC8901489.
25. Petr J, Platzek I, Hofheinz F, et al. Photon vs. proton radiochemotherapy: Effects on brain tissue volume and perfusion. Radiother Oncol 2018;128:121-27.
26. Telischak NA, Detre JA, Zaharchuk G. Arterial spin labeling MRI: clinical applications in the brain. J Magn Reson Imaging 2015;41:1165-80.
27. Detre JA, Rao H, Wang DJ, et al. Applications of arterial spin labeled MRI in the brain. J Magn Reson Imaging 2012;35:1026-37. PMC3326188.
28. Chen Y, Wang DJ, Detre JA. Test-retest reliability of arterial spin labeling with common labeling strategies. J Magn Reson Imaging 2011;33:940-9. PMC3069716.
29. Wu B, Lou X, Wu X, et al. Intra- and interscanner reliability and reproducibility of 3D whole-brain pseudo-continuous arterial spin-labeling MR perfusion at 3T. J Magn Reson Imaging 2014;39:402-9.
30. Xu G, Rowley HA, Wu G, et al. Reliability and precision of pseudo-continuous arterial spin labeling perfusion MRI on 3.0 T and comparison with 15O-water PET in elderly subjects at risk for Alzheimer's disease. NMR Biomed 2010;23:286-93. 2843795.
31. Kilroy E, Apostolova L, Liu C, et al. Reliability of two-dimensional and three-dimensional pseudo-continuous arterial spin labeling perfusion MRI in elderly populations: comparison with 15O-water positron emission tomography. J Magn Reson Imaging 2014;39:931-9. PMC3866214.
32. Zhou L, Wang Y, Pinho MC, et al. Intrasession Reliability of Arterial Spin-Labeled MRI-Measured Noncontrast Perfusion in Glioblastoma at 3 T. Tomography 2020;6:139-47. PMC7289238.
33. Alsaedi AF, Thomas DL, De Vita E, et al. Repeatability of perfusion measurements in adult gliomas using pulsed and pseudo-continuous arterial spin labelling MRI. MAGMA 2021.
34. Bedekar D, Jensen T, Schmainda KM. Standardization of relative cerebral blood volume (rCBV) image maps for ease of both inter- and intrapatient comparisons. Magn Reson Med 2010;64:907-13. PMC4323176.

SUPPLEMENTAL FILES

Supplementary Fig 1. Imaging protocol for healthy volunteers (A) and patients with GBM (B). A) For healthy volunteers, each visit had two imaging sessions with a 15 mins coffee break in between. There were two runs of 3D pCASL with TSE-CASPR and two runs of 3D pCASL with GRASE for each imaging session. B) For GBM patients, two runs of 3D pCASL with TSE- CASPR and at least one run of 3D pCASL with GRASE were included into the existing clinical MR routine protocol.

A) Healthy volunteer protocol	
First session	Second Session
Survey	Survey
3D T1 MP-RAGE	
3D pCASL with TSE-CASPR (Run 1)	3D pCASL with TSE-CASPR (Run 1)
3D pCASL with TSE-CASPR (Run 2)	3D pCASL with TSE-CASPR (Run 2)
3D pCASL with GRASE (Run 1)	3D pCASL with GRASE (Run 1)
3D pCASL with GRASE (Run 2)	3D pCASL with GRASE (Run 2)
...	...
3D T2 FLAIR	
2D T2 TSE	

B) GBM patient protocol
Survey
3D T1 MP-RAGE
3D pCASL with TSE-CASPR (Run 1)
3D pCASL with GRASE (Optional)
3D T2 FLAIR
2D T2 TSE
3D SWI
2D DWI
3D pCASL with TSE-CASPR (Run 2)
3D pCASL with GRASE
2D DCE
2D DSC
3D T1 MP-RAGE (post-contrast)
2D T1 FLAIR (post-contrast)

Supplementary Fig 2. Violin plots of mean perfusion values of grey matter (orange) and white matter (green) from healthy volunteers for both 3D pCASL with TSE-CASPR and 3D pCASL with GRASE. The units of perfusion values are in mL/100g/min.

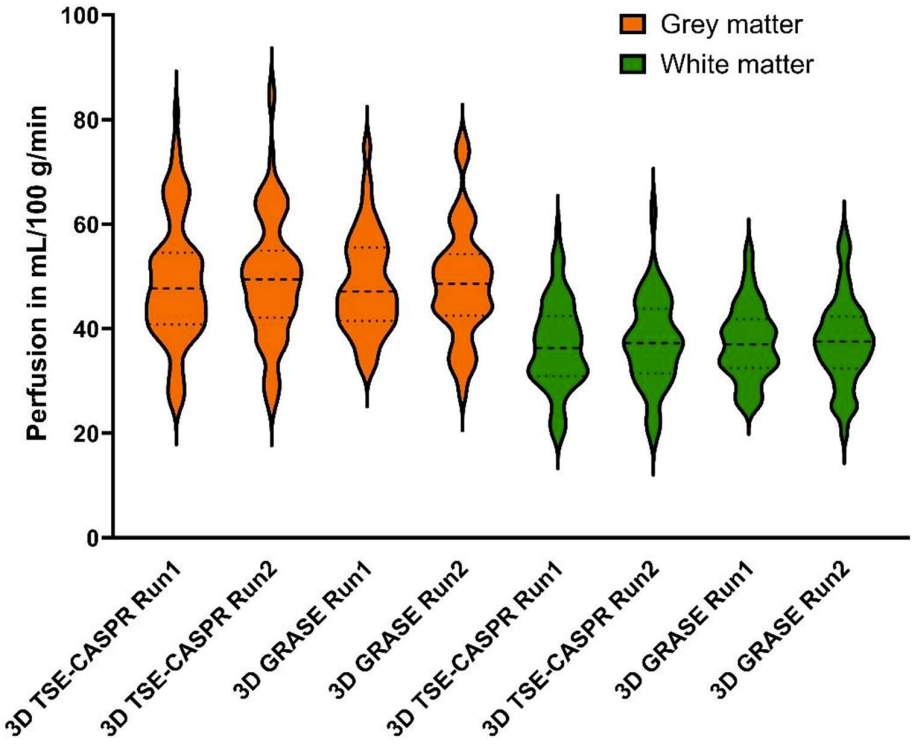

Supplementary Table 1. Linear regression R^2 parameter, intra-class correlation coefficient (ICC) and its 95% confidence interval (CI), and within-subject coefficient variation (wsCV) analyses among mean perfusion values extracted from perfusion maps generated by 3D pCASL with TSE-CASPR and 3D pCASL with GRASE using SRI24 regional ROIs atlas in healthy volunteers.

	TSE-CASPR						GRASE					
	Intra-session			Inter-session			Intra-session			Inter-session		
	R^2	ICC ± 95%CI	wsCV(%)	R^2	ICC ± 95%CI	wsCV(%)	R^2	ICC ± 95%CI	wsCV(%)	R^2	ICC ± 95%CI	wsCV(%)
superior frontal gyrus	0.85	0.92 0.881 - 0.949	6.77	0.57	0.75 0.640 - 0.834	13.96	0.90	0.94 0.914 - 0.964	5.59	0.62	0.78 0.681 - 0.855	11.14
middle frontal gyrus	0.87	0.93 0.894 - 0.955	6.15	0.55	0.73 0.614 - 0.821	13.61	0.89	0.94 0.904 - 0.959	5.66	0.64	0.80 0.697 - 0.865	10.47
inferior frontal gyrus	0.84	0.92 0.872 - 0.945	6.45	0.54	0.73 0.607 - 0.817	13.19	0.84	0.91 0.867 - 0.943	6.62	0.60	0.78 0.670 - 0.849	10.61
precentral gyrus	0.86	0.92 0.874 - 0.949	6.53	0.57	0.75 0.640 - 0.834	13.49	0.85	0.92 0.874 - 0.946	6.58	0.63	0.80 0.700 - 0.864	10.89
middle orbitofrontal gyrus	0.80	0.90 0.843 - 0.932	6.41	0.48	0.68 0.544 - 0.783	12.90	0.75	0.85 0.782 - 0.904	8.34	0.47	0.67 0.535 - 0.778	12.19
lateral orbitofrontal gyrus	0.80	0.89 0.838- 0.930	6.84	0.48	0.68 0.548 - 0.785	13.53	0.77	0.87 0.807- 0.916	8.04	0.44	0.66 0.518 - 0.769	12.89
gyrus rectus	0.55	0.74 0.625 - 0.872	11.25	0.38	0.61 0.458 - 0.733	14.73	0.57	0.74 0.626 - 0.827	10.43	0.28	0.53 0.356 - 0.674	13.93
postcentral gyrus	0.86	0.92 0.871 -0 .947	6.90	0.60	0.77 0.668 - 0.848	13.73	0.87	0.93 0.895 -0 .955	6.66	0.68	0.83 0.742 - 0.885	11.04
superior parietal gyrus	0.87	0.93 0.879 - 0.953	7.26	0.60	0.77 0.667 - 0.848	15.10	0.88	0.93 0.893 - 0.955	6.82	0.69	0.83 0.748 - 0.888	11.74
supramarginal gyrus	0.81	0.90 0.839 - 0.932	8.01	0.58	0.76 0.654 - 0.836	13.81	0.88	0.94 0.903 - 0.959	5.80	0.70	0.83 0.747 - 0.888	9.89
angular gyrus	0.83	0.91 0.864 - 0.942	6.92	0.55	0.74 0.618 - 0.822	13.72	0.89	0.94 0.904 - 0.959	5.49	0.64	0.80 0.699 - 0.864	10.07
precuneus	0.86	0.92 0.883 - 0.950	6.95	0.52	0.71 0.588 - 0.807	15.61	0.89	0.93 0.885 - 0.951	6.34	0.64	0.79 0.682 - 0.860	11.18
superior occipital gyrus	0.77	0.86 0.766 - 0.912	9.40	0.38	0.62 0.460 - 0.737	19.01	0.83	0.89 0.837 - 0.931	7.60	0.55	0.74 0.622- 0.825	13.07
middle occipital gyrus	0.78	0.87 0.796 - 0.920	7.75	0.43	0.66 0.515 - 0.768	15.41	0.84	0.91 0.855 - 0.939	6.74	0.61	0.79 0.658 - 0.857	11.36
inferior occipital gyrus	0.76	0.86 0.770 - 0.909	8.83	0.37	0.61 0.453 - 0.732	18.19	0.78	0.88 0.818 - 0.921	8.60	0.60	0.77 0.669- 0.849	13.11
cuneus	0.86	0.92 0.879 - 0.952	8.49	0.47	0.69 0.553 - 0.788	19.21	0.89	0.93 0.889 - 0.953	7.13	0.67	0.81 0.723 - 0.876	12.49
superior temporal gyrus	0.82	0.91 0.858 - 0.939	6.79	0.52	0.70 0.560 - 0.801	13.79	0.85	0.92 0.871 - 0.945	6.15	0.59	0.75 0.631- 0.836	10.82
middle temporal gyrus	0.85	0.92 0.883 - 0.950	5.85	0.52	0.71 0.576 - 0.802	13.32	0.87	0.93 0.889 - 0.953	5.40	0.63	0.78 0.668 - 0.854	9.67
inferior temporal gyrus	0.84	0.91 0.859 - 0.943	6.83	0.48	0.68 0.543 - 0.783	15.21	0.85	0.91 0.868 - 0.944	7.17	0.71	0.84 0.750 - 0.892	10.10
parahippocampal gyrus	0.85	0.92 0.874 - 0.946	8.59	0.37	0.61 0.454 - 0.731	19.14	0.67	0.82 0.726- 0.877	8.76	0.36	0.59 0.413 - 0.715	13.64
lingual gyrus	0.85	0.92 0.870 - 0.948	8.40	0.47	0.69 0.553 - 0.788	18.28	0.87	0.92 0.874 - 0.946	6.84	0.65	0.81 0.716 - 0.872	11.31
fusiform gyrus	0.78	0.88 0.812 - 0.922	9.59	0.35	0.59 0.425 - 0.715	20.16	0.81	0.89 0.836 - 0.929	8.43	0.60	0.78 0.670 - 0.849	12.74
insular cortex	0.79	0.89 0.830 - 0.926	7.76	0.50	0.70 0.563 - 0.795	13.69	0.79	0.88 0.824 - 0.924	7.90	0.50	0.71 0.582-0.804	12.41
cingulate gyrus	0.79	0.89 0.830 - 0.926	7.32	0.45	0.66 0.522 - 0.771	14.27	0.85	0.91 0.865 - 0.942	6.82	0.49	0.69 0.561 - 0.792	11.98
caudate	0.71	0.84 0.759 - 0.893	7.97	0.39	0.60 0.400 - 0.723	14.19	0.61	0.76 0.655 - 0.842	10.66	0.21	0.45 0.260 - 0.608	15.32
putamen	0.73	0.86 0.785 - 0.905	7.73	0.37	0.59 0.427 - 0.716	14.18	0.63	0.79 0.684 - 0.857	10.77	0.32	0.56 0.385 - 0.690	14.59
hippocampus	0.84	0.91 0.866 - 0.942	7.49	0.42	0.64 0.485 - 0.750	16.46	0.67	0.81 0.720 - 0.874	9.82	0.34	0.57 0.401 - 0.701	14.01
cerebellum	0.82	0.90 0.852 - 0.937	9.32	0.37	0.61 0.452 - 0.730	20.98	0.78	0.88 0.821 - 0.922	9.08	0.60	0.76 0.645 - 0.843	13.13
Mean	0.81	0.89	7.66	0.48	0.68	15.46	0.80	0.89	7.51	0.55	0.73	11.99
SD	**0.07**	**0.04**	**1.23**	**0.08**	**0.06**	**2.43**	**0.09**	**0.06**	**1.59**	**0.14**	**0.10**	**1.50**